

Mott transition and magnetism of the triangular-lattice Hubbard model with next-nearest-neighbor hopping

Kazuma Misumi, Tatsuya Kaneko, and Yukinori Ohta
Department of Physics, Chiba University, Chiba 263-8522, Japan
(Dated: February 1, 2017)

The variational cluster approximation is used to study the isotropic triangular-lattice Hubbard model at half filling, taking into account the nearest-neighbor (t_1) and next-nearest-neighbor (t_2) hopping parameters for magnetic frustrations. We determine the ground-state phase diagram of the model. In the strong correlation regime, the 120° Néel and stripe ordered phases appear, and a nonmagnetic insulating phase emerges in between. In the intermediate correlation regime, the nonmagnetic insulating phase expands to a wider parameter region, which goes into a paramagnetic metallic phase in the weak correlation regime. The critical phase boundary of the Mott metal-insulator transition is discussed in terms of the van Hove singularity evident in the calculated density of states and single-particle spectral function.

PACS numbers: 71.10.Fd 75.10.Jm 71.30.+h 75.10.-b

I. INTRODUCTION

The physics of geometrical frustration in strongly correlated electron systems has long attracted much attention [1–3]. In particular, possible absence of magnetic long-range orders at zero temperature in the Heisenberg and Hubbard models defined on frustrated lattices, or the realization of a spin liquid phase as an exotic state of matter, has been one of the major issues in this field. The Mott metal-insulator transition is also a fundamental phenomenon in the field of strongly correlated electron systems [4, 5], which has attracted much experimental and theoretical interest as well. As one of the simplest models with geometrical frustration and Mott transition, we therefore study the Hubbard model at half filling defined on the triangular lattice in this paper, where not only the nearest-neighbor hopping parameters but also the next-nearest-neighbor ones are included.

Much effort has so far been devoted in the study of the triangular-lattice Hubbard model with *anisotropic* nearest-neighbor hopping parameters [6–14], which was motivated by experimental findings of possible spin liquid states in some organic Mott insulators such as κ -(ET) $_2$ Cu $_2$ (CN) $_3$ [15–18] and EtMe $_3$ Sb[Pd(dmit) $_2$] $_2$ [19, 20]. The triangular-lattice Heisenberg model with the anisotropic exchange interactions has also been studied to find a variety of ordered phases such as Néel and spiral orders, as well as the quantum disordered (or spin liquid) phases in-between [21–23].

However, to the best of our knowledge, the *isotropic* triangular-lattice Hubbard model with both the nearest-neighbor (t_1) and next-nearest-neighbor (t_2) hopping parameters has not yet been addressed, the study of which will therefore provide useful information on the physics of magnetic frustrations and Mott metal-insulator transition in strongly correlated electron systems.

The isotropic Heisenberg model with the nearest-neighbor (J_1) and next-nearest-neighbor (J_2) exchange interactions, which may be derived by the second-order perturbation of the above-mentioned Hubbard model in

the strong correlation limit, has on the other hand been studied much in detail, mostly from the theoretical point of view [24]. In the classical Heisenberg model where the spins are treated as classical vectors, it is known that a single phase transition occurs at $J_2/J_1 = 1/8$ between the three-sublattice 120° Néel ordered state and an infinitely degenerate four-sublattice magnetically ordered states [25]. This degeneracy is lifted by quantum fluctuations, thereby selecting a two-sublattice stripe ordered state through the so-called “order-by-disorder” mechanism [25–28]. One may then expect in the corresponding quantum Heisenberg model that an intermediate phase can appear near the classical critical point at $J_2/J_1 = 1/8$, for which many studies have been carried out to predict that the nonmagnetic disordered phase bordered by the 120° Néel ordered phase at $J_2/J_1 \simeq 0.05 - 0.12$ and the stripe ordered phase at $J_2/J_1 \simeq 0.14 - 0.19$ actually emerges. In particular, recent studies actually predict the emergence of either a gapless or gapped spin liquid phase in this intermediate region [29–35]. These results of the Heisenberg model may be compared with those of our Hubbard model in the strong correlation limit (as we will see below).

In this paper, motivated by the above developments in the field, we will study the triangular-lattice Hubbard model at half filling with the isotropic nearest-neighbor and next-nearest-neighbor hopping parameters in its entire interaction strength. We use the variational cluster approximation (VCA), one of the quantum cluster methods based on the self-energy functional theory (SFT) [36–40], which enables us to take into account the quantum fluctuations of the model with geometrically frustrated spin degrees of freedom. We thereby calculate the grand potential of the system as a function of the Weiss fields for spontaneous symmetry breakings; here, we take the 120° Néel and stripe magnetic orders and evaluate the order parameters and critical interaction strengths. We also calculate the charge gap as well as the density of states (DOS) and single-particle spectral function using the cluster perturbation theory (CPT) [40] and deter-

mine the ground-state phase diagram of the model in its entire parameter region.

We will thereby show that in the strong correlation regime the 120° Néel and stripe ordered phases appear, and in-between, the nonmagnetic insulating phase caused by the quantum fluctuations in the frustrated spin degrees of freedom emerges, in agreement with the Heisenberg model studies. We will also show that in the intermediate correlation regime the nonmagnetic insulating phase expands to wider parameter regions located around $0 \leq t_2/t_1 \lesssim 0.3$ and $0.4 \lesssim t_2/t_1 \leq 1$, which go into a paramagnetic metallic phase in the weak correlation regime via the second-order Mott transition. The characteristic behavior of the critical phase boundary of the Mott transition is discussed in terms of the van Hove singularity appearing in the calculated DOS and single-particle spectral function.

The rest of the paper is organized as follows. In Sec. II, we introduce the model and discuss the method of calculation briefly. In Sec. III A, we present our results obtained in the strong correlation regime and compare them with those of the Heisenberg model. In Sec. III B, we present our results obtained in the intermediate to weak correlation regime and discuss the phase diagram of our model. The critical phase boundary of the Mott transition is also discussed. A summary of the paper is given in Sec. IV.

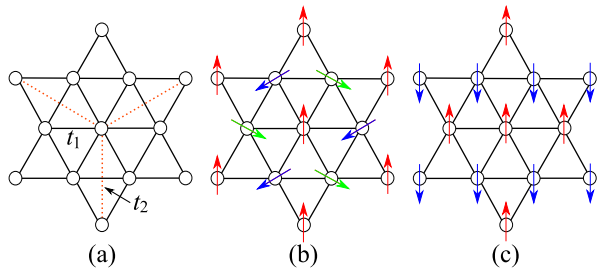


FIG. 1. (Color online) Schematic representations of (a) the triangular-lattice Hubbard model with the nearest-neighbor (t_1) and next-nearest-neighbor (t_2) hopping parameters, (b) the 120° Néel order, and (c) the stripe order. The arrows represent the directions of electron spins on the A, B, and C sublattices defined by different colors.

II. MODEL AND METHOD

We consider the triangular-lattice Hubbard model [see Fig. 1(a)] defined by the Hamiltonian

$$H = -t_1 \sum_{\langle i,j \rangle} \sum_{\sigma} c_{i\sigma}^{\dagger} c_{j\sigma} - t_2 \sum_{\langle\langle i,j \rangle\rangle} \sum_{\sigma} c_{i\sigma}^{\dagger} c_{j\sigma} + U \sum_i n_{i\uparrow} n_{i\downarrow} - \mu \sum_{i,\sigma} n_{i\sigma}, \quad (1)$$

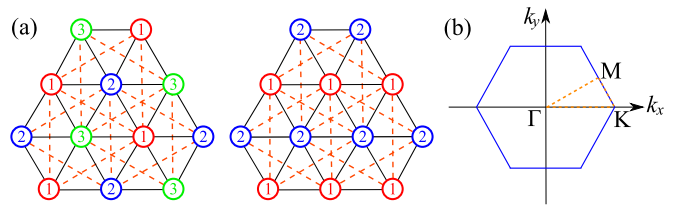


FIG. 2. (Color online) (a) The reference system of the 12-site cluster used in our analysis; the three-sublattice system corresponding to the 120° Néel order (left) and the two-sublattice system corresponding to the stripe order (right). (b) The first Brillouin zone of our triangular-lattice Hubbard model: $\Gamma(0, 0)$, $K(4\pi/3, 0)$, and $M(\pi, \pi/\sqrt{3})$.

where $c_{i\sigma}^{\dagger}$ ($c_{i\sigma}$) creates (annihilates) an electron with spin σ at site i , and $n_{i\sigma} = c_{i\sigma}^{\dagger} c_{i\sigma}$. $\langle i, j \rangle$ indicates the nearest-neighbor bonds with the hopping parameter t_1 and $\langle\langle i, j \rangle\rangle$ indicates the next-nearest-neighbor bonds with the hopping parameter t_2 . We consider the parameter region $0 \leq t_2/t_1 \leq 1$, including two limiting cases, $t_2 = 0$ (isotropic triangular lattice) and $t_2 = t_1$. U is the on-site Coulomb repulsion between two electrons and μ is the chemical potential maintaining the system at half filling.

In the large- U limit, this model may be mapped onto the triangular-lattice Heisenberg model of spin-1/2 defined by the Hamiltonian

$$H = J_1 \sum_{\langle i,j \rangle} \mathbf{S}_i \cdot \mathbf{S}_j + J_2 \sum_{\langle\langle i,j \rangle\rangle} \mathbf{S}_i \cdot \mathbf{S}_j \quad (2)$$

with the exchange coupling constants of $J_1 = 4t_1^2/U$ and $J_2 = 4t_2^2/U$ for the nearest-neighbor and next-nearest-neighbor bonds, respectively. The spin operator is given by $\mathbf{S}_i = \sum_{\alpha\beta} c_{i\alpha}^{\dagger} \boldsymbol{\sigma}_{\alpha\beta} c_{i\beta} / 2$ with the vector of Pauli matrices $\boldsymbol{\sigma}_{\alpha\beta}$. The results obtained for the Hubbard model [Eq. (1)] in the strong correlation regime are compared with those of the Heisenberg model [Eq. (2)].

Let us describe the VCA briefly, which is a many-body variational method based on the SFT, where the grand potential of the system is formulated as a functional of the self-energy [36–38]. The ground state of the original system in the thermodynamic limit can thus be obtained via the calculation of the grand potential Ω of the system with the exact self-energy. Then, in the VCA, restricting the trial self-energy to the self-energy of the reference system Σ' , we obtain the approximate grand potential as

$$\Omega[\Sigma'] = \Omega' + \text{Trln}(G_0^{-1} - \Sigma')^{-1} - \text{Trln}(G_0'^{-1} - \Sigma')^{-1}, \quad (3)$$

where Ω' is the grand potential of the reference system, and G_0 and G_0' are the noninteracting Green's functions of the original and reference systems, respectively. The Hamiltonian of the reference system H' is defined below. Note that the short-range correlations within the clusters of the reference system are taken into account exactly. See Refs. 39 and 40 for recent reviews of the method.

The advantage of the VCA is that the spontaneous symmetry breaking can be treated within the framework of the theory, where we introduce the Weiss fields as variational parameters. In the present case, the Hamiltonian of the reference system is taken as $H' = H + H_M$ with the Weiss fields

$$H_M = H_{120^\circ} + H_{\text{str}} \quad (4)$$

$$H_{120^\circ} = h'_{120^\circ} \sum_i \mathbf{e}_{a_i} \cdot \mathbf{S}_i \quad (5)$$

$$H_{\text{str}} = h'_{\text{str}} \sum_i e^{i\mathbf{Q}_{\text{str}} \cdot \mathbf{r}_i} S_i^z, \quad (6)$$

where h'_{120° and h'_{str} are the strengths of the Weiss fields for the 120° Néel and stripe ordered states, respectively. For the Néel order, the unit vectors \mathbf{e}_{a_i} are rotated by 120° to each other, where a_i ($= 1, 2, 3$) is the sublattice index of site i . For the stripe order, the wave vectors can be taken equivalently as either $\mathbf{Q}_{\text{str}} = (\pi, \pi/\sqrt{3})$, $(\pi, -\pi/\sqrt{3})$, or $(0, -2\pi/\sqrt{3})$. The variational parameters are optimized on the basis of the variational principle, i.e., $\partial\Omega/\partial h' = 0$, for each magnetic order, where the solution with $h' \neq 0$ corresponds to the ordered state.

In our VCA calculations, we use the 12-site cluster shown in Fig. 2 as the reference system. This is the best appropriate and feasible choice of the reference cluster because we can treat the two-sublattice order (stripe order) with an equal number of up- and down-spin electrons and the three-sublattice order (120° Néel order) with an equal number of the three sublattice sites $a_i = 1, 2$ and 3 . The cluster-size and cluster-shape dependences of our results are discussed in Appendix. Note that longer period phases such as the spiral phase mentioned in a different system [11] cannot be treated in the present approach; in our analysis, we fix the pitch angle of the spiral order to be 120° (or the three-sublattice of $a_i = 1, 2, 3$) even for $t_2 \neq 0$. The charge orderings discussed in the extended Hubbard model with intersite Coulomb repulsions [41] are also neglected. To our knowledge, no other orders have been predicted in the present triangular-lattice Hubbard and Heisenberg models.

III. RESULTS OF CALCULATION

A. Strong correlation regime

First, let us discuss the strong correlation regime, $U/t_1 = 60$. We calculate the ground-state energies $E = \Omega + \mu$ (per site) and magnetic order parameters M defined as $M_{120^\circ} = (2/L) \sum_i \mathbf{e}_{a_i} \cdot \langle \mathbf{S}_i \rangle$ for the 120° Néel order and $M_{\text{str}} = (2/L) \sum_i e^{i\mathbf{Q}_{\text{str}} \cdot \mathbf{r}_i} \langle S_i^z \rangle$ for the stripe order, where $\langle \dots \rangle$ stands for the ground-state expectation value. The results are shown in Fig. 3, where we find three phases: the 120° Néel ordered phase around $t_2/t_1 = 0$, the stripe ordered phase around $t_2/t_1 = 1$, and the nonmagnetic disordered phase in-between.

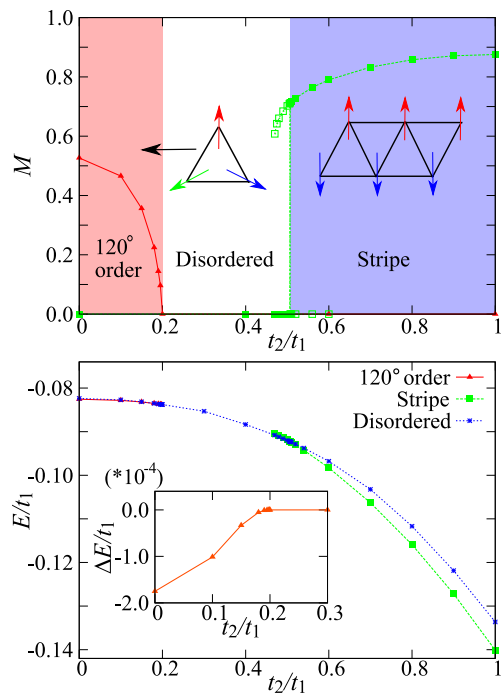


FIG. 3. (Color online) Calculated ground-state phase diagram of our model in the strong correlation regime ($U/t_1 = 60$). Upper panel: the order parameters of the 120° Néel and stripe ordered phases. Solid (open) symbols indicate that the state is stable (metastable). Lower panel: the ground-state energies (per site) of the ordered phases compared with that of the disordered phase. Inset shows the enlargement of the energy difference ΔE between the 120° ordered and disordered phases.

At $t_2/t_1 = 0$, the 120° Néel ordered state has the lowest energy and with increasing t_2/t_1 it approaches the energy of the nonmagnetic disordered state gradually. Then, at $t_2/t_1 = 0.20$, the 120° Néel ordered state disappears continuously. The calculated order parameter M_{120° also indicates the continuous (or second-order) phase transition. On the other hand, at $t_2/t_1 = 1.0$, the stripe ordered state has the lowest energy and, with decreasing t_2/t_1 , the energy of stripe order crosses to that of the nonmagnetic state at $t_2/t_1 = 0.50$, indicating the discontinuous (or first-order) transition between the stripe and disordered phases. The calculated order parameter M_{str} also disappears discontinuously at $t_2/t_1 = 0.50$.

These results may be compared with the previous studies on the J_1 - J_2 triangular-lattice Heisenberg model [29–34]. The transition point between the 120° Néel and nonmagnetic phases has been estimated to be $J_2/J_1 = 0.05 - 0.12$, which corresponds to $t_2/t_1 = 0.22 - 0.35$ of our Hubbard model parameters. A reasonable agreement is thus obtained. The transition point between the stripe and nonmagnetic phases has also been estimated to be $J_2/J_1 = 0.14 - 0.19$, which corresponds to $t_2/t_1 = 0.37 - 0.44$ of our Hubbard model parameters. We again find a reasonable agreement with our estimation.

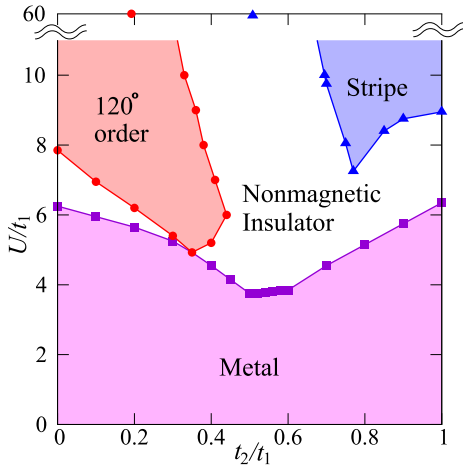


FIG. 4. (Color online) Calculated ground-state phase diagram of our model in the intermediate to weak correlation regime, which includes the 120° Néel ordered, stripe ordered, nonmagnetic insulating, and paramagnetic metallic phases. Circle and triangle at $U/t_1 = 60$ indicate the calculated phase boundaries of the 120° Néel order and stripe order, respectively, shown in Fig. 3.

The orders of the phase transitions, i.e., the second-order for the 120° Néel phase and the first-order for the stripe phase, are also in agreement with the previous study of the Heisenberg model [31]. We may point out that the strong quantum fluctuations in the frustrated spin degrees of freedom causes this nonmagnetic phase because the classical spin model predicts either the 120° Néel or four-sublattice ordered phase without any intermediate nonmagnetic phases [25–28].

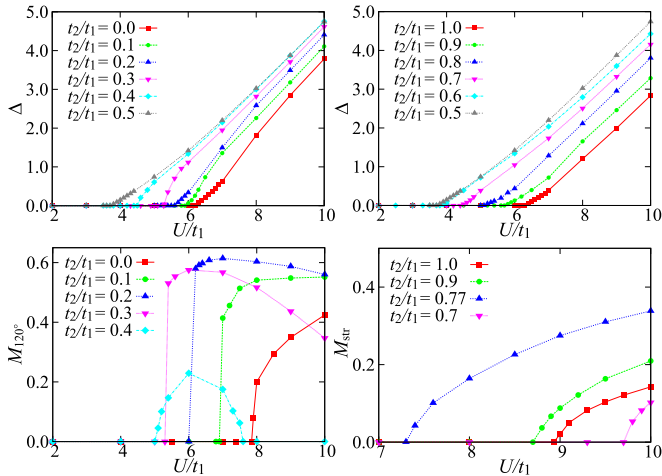


FIG. 5. (Color online) Calculated charge gap Δ (upper panels) and order parameters M_{120° and M_{str} (lower panels) of our model as a function of U/t_1 .

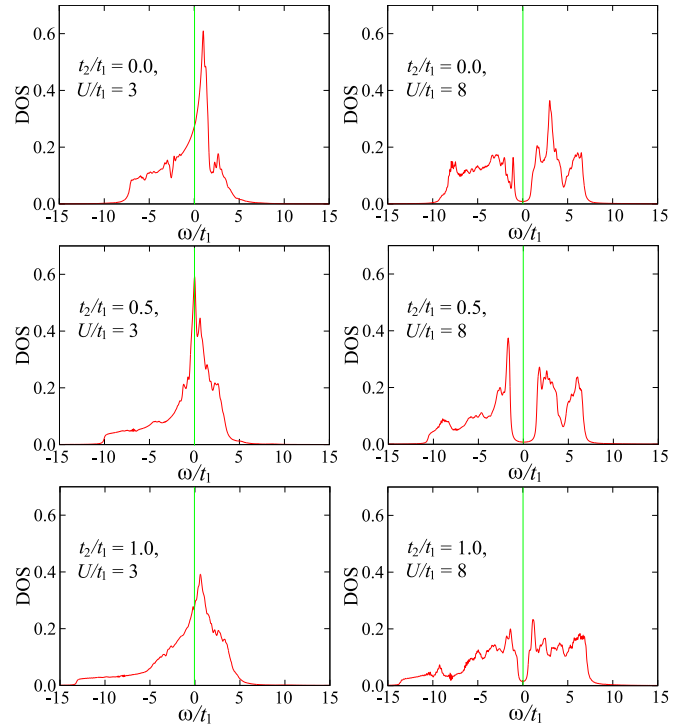


FIG. 6. (Color online) Calculated DOSs of our model in the metallic state (left panels) and insulating state without long-range magnetic orders (right panels). $\eta/t_1 = 0.1$ is assumed. The vertical line in each panel indicates the Fermi level.

B. Intermediate to weak correlation regime

Next, let us discuss the intermediate to weak correlation regime $0 \leq U/t_1 \leq 10$. We here calculate the total energies, order parameters, and charge gaps of the model, as well as the grand potential as a function of the Weiss fields, and summarize them as the ground-state phase diagram in the parameter space $(t_2/t_1, U/t_1)$, as shown in Fig. 4. We find four phases: the 120° Néel and stripe ordered phases at large U/t_1 , which are continuous to the phases at $U/t_1 = 60$ discussed above, and nonmagnetic insulating phase in-between, as well as the paramagnetic metallic phase in the weak correlation regime. In the intermediate correlation regime, the nonmagnetic insulating phase expands to wider parameter regions, which are around $0 \leq t_2/t_1 \lesssim 0.3$ and around $0.4 \lesssim t_2/t_1 \leq 1$. We note that the presence of the nonmagnetic insulating phase around $0 \leq t_2/t_1 \lesssim 0.3$ is in agreement with previous studies of the triangular-lattice Hubbard model at $t_2/t_1 = 0$ [12, 13, 42–44].

The calculated order parameters of the 120° Néel and stripe phases are shown in Fig. 5 as a function of U/t_1 for several values of t_2/t_1 . We find that the transition to the stripe ordered phase is continuous, irrespective of t_2/t_1 , up to a large value of $U/t_1 \sim 30$, but it changes to the discontinuous transition as seen in Fig. 3 at $U/t_1 = 60$. We also find that the transition to the 120° Néel ordered

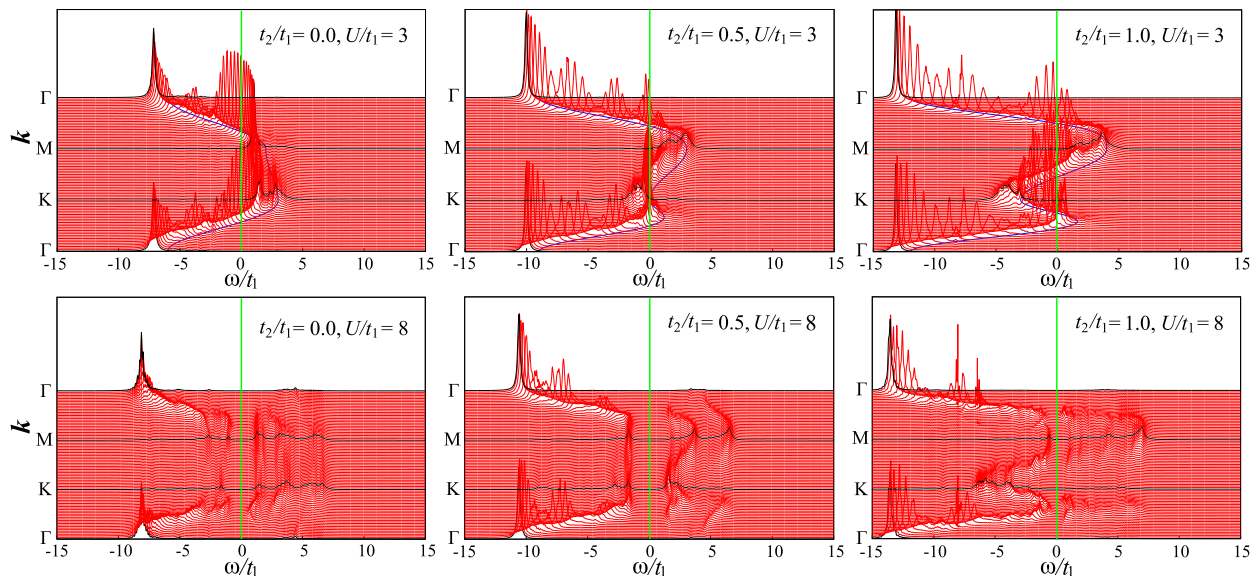


FIG. 7. (Color online) Calculated single-particle spectral function $A(\mathbf{k}, \omega)$ in the paramagnetic state of our model. The wave vector \mathbf{k} is chosen along the line connecting Γ , K, and M points of the Brillouin zone [see Fig. 2 (b)]. $\eta/t_1 = 0.1$ is assumed. The noninteracting band dispersion is also shown by a thin solid curve in each of the upper panels. The Fermi level (indicated by the vertical line) is set at $\omega/t_1 = 0$.

phase is discontinuous at $0 < t_2/t_1 \leq 0.35$ for $U/t_1 \simeq 6$ but it is continuous for larger values of U/t_1 . The transition at $U/t_1 = 60$ is also continuous (see Fig. 3). These behaviors are observed also in the calculated Weiss-field dependence of the grand potentials of our model.

The charge gap is evaluated from the total number of electrons as a function of μ (see Fig. 5) to examine the Mott metal-insulator transition of the system. We find that the transition is continuous (or second-order) and the phase boundary is located around $U/t_1 \simeq 4 - 6$, as shown in Fig. 4. We note that the phase boundary decreases (shifts to a lower U/t_1 side) with increasing t_2/t_1 up to $t_2/t_1 \simeq 0.5$, but it increases for larger values of t_2/t_1 . This behavior is in contrast to that of the square-lattice Hubbard model with the next-nearest-neighbor hopping parameters, where a monotonous increase in the critical interaction strength is observed [45–47], which is due to the monotonous increase in the band width of the model.

To find out the origin of this behavior, we calculate the DOS $\rho(\omega)$ and single-particle spectral function $A(\mathbf{k}, \omega)$ in the paramagnetic state of the system using the CPT, which are defined as

$$\rho(\omega) = \frac{1}{L} \sum_{\mathbf{k}} A(\mathbf{k}, \omega) \quad (7)$$

$$A(\mathbf{k}, \omega) = -\frac{1}{\pi} \lim_{\eta \rightarrow 0} \Im \mathcal{G}_{\text{CPT}}(\mathbf{k}, \omega + i\eta) \quad (8)$$

with the CPT Green's function [40]

$$\mathcal{G}_{\text{CPT}}(\mathbf{k}, \omega) = \frac{1}{L_c} \sum_{i,j=1}^{L_c} \mathcal{G}_{ij}(\mathbf{k}, \omega) e^{-i\mathbf{k} \cdot (\mathbf{r}_i - \mathbf{r}_j)}, \quad (9)$$

where we define the $L_c \times L_c$ matrices for the cluster of size L_c as $\mathcal{G}(\mathbf{k}, \omega) = [G'^{-1}(\omega) - V(\mathbf{k})]^{-1}$ with $V(\mathbf{k}) = G_0'^{-1} - G_0^{-1}$. The exact Green's function of the reference system $G'(\omega)$ is given by

$$G'_{ij}(\omega) = \langle \psi_0 | c_{i\sigma} \frac{1}{\omega - H' + E_0} c_{j\sigma}^\dagger | \psi_0 \rangle + \langle \psi_0 | c_{j\sigma}^\dagger \frac{1}{\omega + H' - E_0} c_{i\sigma} | \psi_0 \rangle, \quad (10)$$

where $|\psi_0\rangle$ and E_0 are the ground state and ground state energy of H' .

The calculated results for the DOS and single-particle spectral function of our model are shown in Figs. 6 and 7, respectively. We find that the sharp peak appeared above the Fermi level at $t_2/t_1 = 0$, which is caused by the van Hove singularity in the triangular lattice, shifts to the lower energy side with increasing t_2/t_1 , and at $t_2/t_1 = 0.5$, the peak position coincides with the Fermi level (see Fig. 6). This situation of the high DOS at the Fermi level is energetically unstable [48], so that the band gap opens to gain in the band energy in the presence of the Hubbard interaction U . With further increasing t_2/t_1 , the peak shifts to the higher energy side again. The Hubbard band gap is then the largest at $t_2/t_1 = 0.5$ as seen in Figs. 5 and 6. This singularity is also seen in the single-particle spectral function as the presence of the

flat-band region around the K point of the Brillouin zone (see Fig. 7). This behavior thus explains why the critical interaction strength becomes small at around $t_2/t_1 \simeq 0.5$.

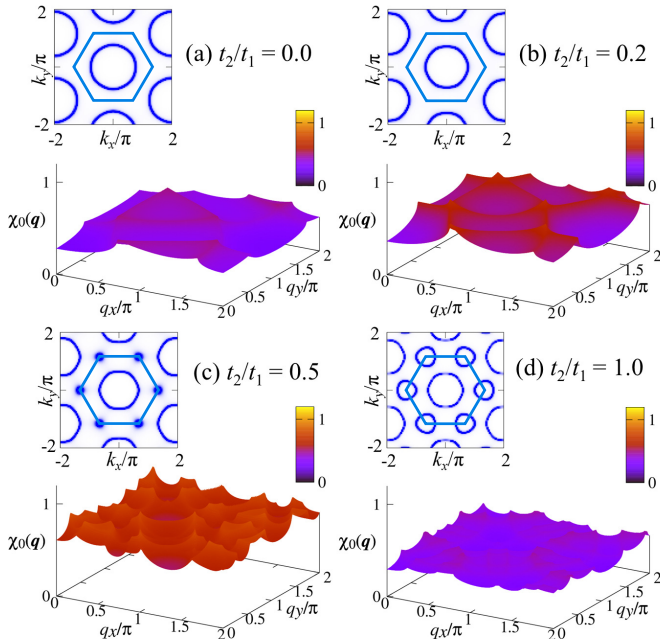


FIG. 8. (Color online) Calculated generalized magnetic susceptibility in the noninteracting limit $\chi_0(\mathbf{q})$ defined in Eq. (11). The corresponding Fermi surface is shown in each panel, where the first Brillouin zone is indicated by a hexagon.

To confirm the absence of any magnetic instability in our model in the weak correlation regime, we here calculate the generalized susceptibility (or Lindhard function) in the noninteracting limit, which is defined as

$$\chi_0(\mathbf{q}) = \frac{1}{L} \sum_{\mathbf{k}} \frac{f(\varepsilon_{\mathbf{k}}) - f(\varepsilon_{\mathbf{k}+\mathbf{q}})}{\varepsilon_{\mathbf{k}+\mathbf{q}} - \varepsilon_{\mathbf{k}}}, \quad (11)$$

where $\varepsilon_{\mathbf{k}}$ is the corresponding noninteracting band dispersion and $f(\varepsilon)$ is the Fermi function. The calculated results at temperature $0.01t_1$ are shown in Fig. 8, where we find that, in accordance with the absence of significant Fermi-surface nesting features, no singular behaviors actually appear in $\chi_0(\mathbf{q})$, indicating the absence of magnetic long-range orders in the weak correlation limit. This result supports the validity of our phase diagram shown in Fig. 4 in the weak correlation regime.

IV. SUMMARY

We have studied the Mott metal-insulator transition and magnetism of the triangular-lattice Hubbard model at half filling in the entire region of the interaction strength, taking into account the next-nearest-neighbor hopping parameters for the effects of magnetic frustrations. We have employed the method of VCA based on

the SFT, which has not been used for the present purposes. We have thereby calculated the grand potential of the system as a function of the Weiss fields for the 120° Néel and stripe magnetic orders, and have determined the order parameters. We have also calculated the DOS and single-particle spectral function as well as the charge gap of the system. These results have been summarized as the ground-state phase diagram of the system.

We have found four phases: In the strong correlation regime, there appear (i) the 120° Néel ordered phase in a wide parameter region around $t_2/t_1 \simeq 0$ and (ii) the stripe ordered phase in a wide parameter region around $t_2/t_1 \simeq 1$, and in-between, (iii) the nonmagnetic insulating phase caused by the quantum fluctuations in the geometrically frustrated spin degrees of freedom emerges. The obtained phase boundaries in the strong correlation limit have been compared with those of the corresponding Heisenberg model to find a reasonable agreement. The orders of the phase transitions of the two magnetically ordered phases have also been determined. In the intermediate correlation regime, the nonmagnetic insulating phase expands to a wider parameter region of t_2/t_1 . Then, decreasing the interaction strength further, the system turns into (iv) the paramagnetic metallic phase in the weak correlation regime via the second-order Mott metal-insulator transition. The characteristic behavior of the critical phase boundary of the Mott transition has also been discussed in terms of the shift in the van Hove singularity due to the presence of t_2 , as seen in the calculated DOS and single-particle spectral function.

We suggest that the phase diagram obtained here may contain different types of nonmagnetic insulator (or spin liquid) states depending on the region in the parameter space. The characterization of the states is however beyond the scope of the VCA approach based on the self-energy (or single-particle Green's function), for which we hope that our results will encourage future studies.

ACKNOWLEDGMENTS

We thank S. Miyakoshi for enlightening discussions and K. Seki for careful reading of our manuscript. This work was supported in part by a Grant-in-Aid for Scientific Research (No. 26400349) from JSPS of Japan. T. K. acknowledges support from the JSPS Research Fellowship for Young Scientists.

Appendix: Cluster dependence of the phase boundaries

In the VCA, or in any other quantum cluster methods, we can in principle calculate the physical quantities in the thermodynamic limit, but the calculated results necessarily depend on the size and shape of the solver cluster. Thus, the choice of the solver cluster is important in the present approach. In the main text, we have

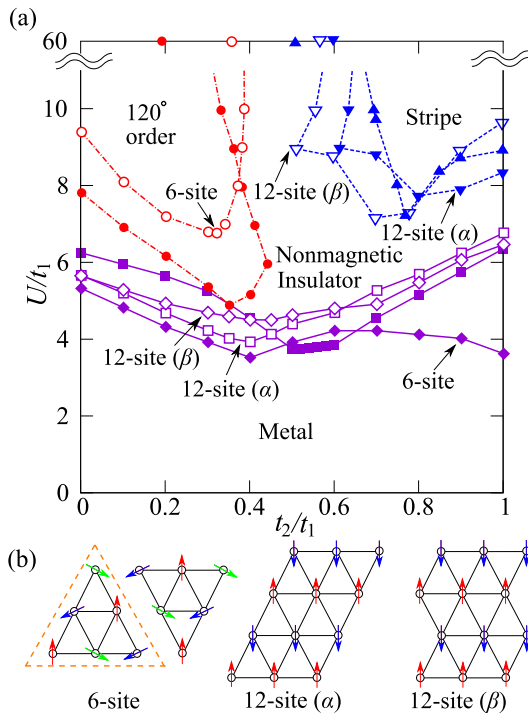


FIG. 9. (Color online) (a) Cluster-size and cluster-shape dependences of the phase boundaries between the 120° Néel ordered, stripe ordered, nonmagnetic insulating, and paramagnetic metallic phases. Unlabeled lines are the results shown in Fig. 4. (b) Schematic representations of the clusters used in the calculations; in the 6-site cluster calculation, we combine two of them to reproduce the 120° Néel order.

chosen the 12-site cluster shown in Fig. 2, which is the best appropriate one because it is first of all computationally feasible and also because it fits with both the three-sublattice 120° order and two-sublattice stripe order without introducing unnecessary frustrations. However, it seems instructive to check the cluster-size and cluster-shape dependences of our results presented in the main text.

Here, we choose several clusters [see Fig. 9(b)] that fit either with the 120° order or with the stripe order, and we calculate the phase boundaries to check the solver cluster dependence of the ground-state phase diagram shown in Fig. 4. The calculated results for the phase boundaries are shown in Fig. 9(a). We thus find that the phase boundary between the 120° Néel ordered and nonmagnetic insulating phases is located around $0 \lesssim t_2/t_1 \lesssim 0.4$ in an intermediate to large U/t_1 ($\gtrsim 6$) region and that the phase boundary between the stripe ordered and nonmagnetic insulating phases is located around $0.5 \lesssim t_2/t_1 \leq 1$ in an intermediate to large U/t_1 ($\gtrsim 7$) region, irrespective of the appropriate choices of the solver cluster. We also find that the phase boundary of the Mott metal-insulator transition is located around $U/t_1 \simeq 4 - 6$ with a minimum at $t_2/t_1 \simeq 0.5$, irrespective of the choices of the solver cluster.

- [1] P. Anderson, Mater. Res. Bull. **8**, 153 (1973).
- [2] L. Balents, Nature (London) **464**, 199 (2010).
- [3] P. A. Lee, N. Nagaosa, and X.-G. Wen, Rev. Mod. Phys. **78**, 17 (2006).
- [4] N. Mott, *Metal-Insulator Transitions* (Taylor and Francis, London, UK, 1990).
- [5] M. Imada, A. Fujimori, and Y. Tokura, Rev. Mod. Phys. **70**, 1039 (1998).
- [6] H. Morita, S. Watanabe, and M. Imada, J. Phys. Soc. Jpn. **71**, 2109 (2002).
- [7] P. Sahebsara and D. Sénéchal, Phys. Rev. Lett. **97**, 257004 (2006).
- [8] T. Watanabe, H. Yokoyama, Y. Tanaka, and J. Inoue, Phys. Rev. B **77**, 214505 (2008).
- [9] T. Ohashi, T. Momoi, H. Tsunetsugu, and N. Kawakami, Phys. Rev. Lett. **100**, 076402 (2008).
- [10] L. F. Tocchio, A. Parola, C. Gros, and F. Becca, Phys. Rev. B **80**, 064419 (2009).
- [11] L. F. Tocchio, H. Feldner, F. Becca, R. Valentini, and C. Gros, Phys. Rev. B **87**, 035143 (2013).
- [12] A. Yamada, Phys. Rev. B **89**, 195108 (2014).
- [13] M. Laubach, R. Thomale, C. Platt, W. Hanke, and G. Li, Phys. Rev. B **91**, 245125 (2015).
- [14] K. Misumi, T. Kaneko, and Y. Ohta, J. Phys. Soc. Jpn., in press (2016).
- [15] T. Komatsu, N. Matsukawa, T. Inoue, and G. Saito, J. Phys. Soc. Jpn. **65**, 1340 (1996).
- [16] Y. Shimizu, K. Miyagawa, K. Kanoda, M. Maesato, and G. Saito, Phys. Rev. Lett. **91**, 107001 (2003).
- [17] Y. Kurosaki, Y. Shimizu, K. Miyagawa, K. Kanoda, and G. Saito, Phys. Rev. Lett. **95**, 177001 (2005).
- [18] R. S. Manna, M. de Souza, A. Brühl, J. A. Schlueter, and M. Lang, Phys. Rev. Lett. **104**, 016403 (2010).
- [19] T. Itou, A. Oyamada, S. Maegawa, M. Tamura, and R. Kato, Phys. Rev. B **77**, 104413 (2008).
- [20] M. Yamashita, N. Nakata, Y. Senshu, M. Nagata, H. M. Yamamoto, R. Kato, T. Shibauchi, and Y. Matsuda, Science **328**, 1246 (2010).
- [21] Z. Weihong, R. H. McKenzie, and R. R. P. Singh, Phys. Rev. B **59**, 14367 (1999).
- [22] P. Hauke, T. Roscilde, V. Murg, J. Cirac, and R. Schmied, New J. Phys. **13**, 075017 (2011).
- [23] P. Hauke, Phys. Rev. B **87**, 014415 (2013).
- [24] A rare exception is $\text{Ba}_3\text{CoSb}_2\text{O}_9$, which was reported to be an almost perfect realization of a spin-1/2 equilateral triangular-lattice antiferromagnet. See, e.g., J. Ma, Y. Kamiya, T. Hong, H. B. Cao, G. Ehlers, W. Tian, C. D. Batista, Z. L. Dun, H. D. Zhou, and M. Matsuda, Phys. Rev. Lett. **116**, 087201 (2016).

- [25] T. Jolicoeur, E. Dagotto, E. Gagliano, and S. Bacci, Phys. Rev. B **42**, 4800 (1990).
- [26] A. V. Chubukov and T. Jolicoeur, Phys. Rev. B **46**, 11137 (1992).
- [27] R. Deutscher and H. U. Everts, Z. Phys. B **93**, 77 (1993).
- [28] P. Lecheminant, B. Bernu, C. Lhuillier, and L. Pierre, Phys. Rev. B **52**, 6647 (1995).
- [29] L. O. Manuel and H. A. Ceccatto, Phys. Rev. B **60**, 9489 (1999).
- [30] R. V. Mishmash, J. R. Garrison, S. Bieri, and C. Xu, Phys. Rev. Lett. **111**, 157203 (2013).
- [31] R. Kaneko, S. Morita, and M. Imada, J. Phys. Soc. Jpn. **83**, 093707 (2014).
- [32] P. H. Y. Li, R. F. Bishop, and C. E. Campbell, Phys. Rev. B **91**, 014426 (2015).
- [33] Z. Zhu and S. R. White, Phys. Rev. B **92**, 041105 (2015).
- [34] W.-J. Hu, S.-S. Gong, W. Zhu, and D. N. Sheng, Phys. Rev. B **92**, 140403 (2015).
- [35] Y. Iqbal, W.-J. Hu, R. Thomale, D. Poilblanc, and F. Becca, Phys. Rev. B **93**, 144411 (2016).
- [36] M. Potthoff, M. Aichhorn, and C. Dahnken, Phys. Rev. Lett. **91**, 206402 (2003).
- [37] M. Potthoff, Eur. Phys. J. B **32**, 429 and **36** 335 (2003).
- [38] C. Dahnken, M. Aichhorn, W. Hanke, E. Arrighoni, and M. Potthoff, Phys. Rev. B **70**, 245110 (2004).
- [39] M. Potthoff, in *Strongly Correlated Systems—Theoretical Methods*, Vol. 171 of Springer Series in Solid-State Sciences (Springer-Verlag, Berlin Heidelberg, 2012), Chap. 10, pp. 303–339.
- [40] D. Sénéchal, in *Strongly Correlated Systems—Theoretical Methods*, Vol. 171 of Springer Series in Solid-State Sciences (Springer-Verlag, Berlin Heidelberg, 2012), Chap. 8, pp. 237–270.
- [41] L. F. Tocchio, C. Gros, X.-F. Zhang, and S. Eggert, Phys. Rev. Lett. **113**, 246405 (2014).
- [42] P. Sahebsara and D. Sénéchal, Phys. Rev. Lett. **100**, 136402 (2008).
- [43] T. Yoshioka, A. Koga, and N. Kawakami, Phys. Rev. Lett. **103**, 036401 (2009).
- [44] T. Yoshioka, A. Koga, and N. Kawakami, Phys. Stat. Sol. (b) **247**, 635 (2010).
- [45] T. Mizusaki and M. Imada, Phys. Rev. B **74**, 014421 (2006).
- [46] A. H. Nevidomskyy, C. Scheiber, D. Sénéchal, and A. -M. S. Tremblay, Phys. Rev. B **77**, 064427 (2008).
- [47] A. Yamada, K. Seki, R. Eder, and Y. Ohta, Phys. Rev. B **88**, 075114 (2013).
- [48] P. Fazekas, *Lecture Notes on Electron Correlation and Magnetism*, Vol. 5 of Series in Modern Condensed Matter Physics (World Scientific, Singapore, 1999).